Optics Communications 396 (2017) 160–168

Contents lists available at ScienceDirect

Optics Communications

journal homepage: www.elsevier.com/locate/optcom

A 3-D high accuracy positioning system based on visible light communication with novel positioning algorithm

Huanhuan Zheng[a,b,*], Zhaowen Xu[b], Changyuan Yu[a,c], Mohan Gurusamy[a]

[a] Department of Electrical and Computer Engineering, National University of Singapore, 117576, Singapore
[b] A*STAR Institute for Infocomm Research (I2R), 138632, Singapore
[c] Department of Electronic and Information Engineering, The Hong Kong Polytechnic University, China

ARTICLE INFO

Keywords:
Visible light positioning
Error correcting algorithm
Positioning error

ABSTRACT

A novel indoor positioning system (IPS) with high positioning precision, based on visible light communication (VLC), is proposed and demonstrated with the dimensions of 100 cm×118.5 cm×128.7 cm. The average positioning distance error is 1.72 cm using the original 2-D positioning algorithm. However, at the corners of the test-bed, the positioning errors are relatively larger than other places. Thus, an error correcting algorithm (ECA) is applied at the corners in order to improve the positioning accuracy. The average positioning errors of four corners decrease from 3.67 cm to 1.55 cm. Then, a 3-D positioning algorithm is developed and the average positioning error of 1.90 cm in space is achieved. Four altitude levels are chosen and on each receiver plane with different heights, four points are picked up to test the positioning error. The average positioning errors in 3-D space are all within 3 cm on these four levels and the performance on each level is similar. A random track is also drawn to show that in 3-D space, the positioning error of random point is within 3 cm.

1. Introduction

Indoor localization has becoming an emerging and attractive area in the past two decades. There is an increasing demand for navigation-based applications. The navigation system called Global Positioning System (GPS) has been well established for the outdoor scenarios. GPS has being widely used, not only for locating users' position, but also tracking paths of mobile users. GPS is a satellite-based system, whose positioning accuracy is in the order of several meters [1]. However, its performance is actually limited when applying in indoor environments because of the significant power attenuation when satellite signals passing through walls of large buildings. This leads to the unacceptable large positioning errors when GPS is used as an indoor navigation system.

For indoor scenarios, various positioning systems have been proposed to circumvent this situation. Some systems use existing infrastructure like Wi-Fi-based system, thus save cost, but their positioning accuracy is not good enough (1–5 m) [1]. Some systems have good positioning accuracy such as ultra-wideband (UWB) systems. However, they are costly. Besides, some other positioning systems like cellular-based systems realize navigation at the base station, which raises privacy concerns for users [2]. The comparison of some positioning systems based on RF signals is given in [1–3].

Recently, the conventional bulbs are replaced by light emitting diodes (LEDs), due to its long life time, high tolerance to humidity, energy efficiency, and ecologically friendly. As we know, the LEDs have other functions beyond illumination, such as data communication and localization. Applications based on visible light communication (VLC) can be used in many areas, such as communication in hazardous or RF sensitive environment, location based service, vehicle and transportation applications [3,4]. The positioning system using LEDs becomes promising since there is no extra installation cost and no electromagnetic interference. Positioning scheme based on VLC can be used for location tracking, controlling robot movement, finding objects, and so on. In this article, LED lights are proposed to be used as the positioning sensors in order to set up the indoor localization system and propose a positioning technique by assigning different carrier frequencies to different LEDs at transmitter side and applying Hamming filter to distinguish them at receiver side.

Some main ranging techniques, which are reported to be put into use in VLC positioning systems, include received signal strength (RSS), time difference of arrival (TDOA), and phase difference of arrival (PDOA) [4,5]. However, for those systems using TDOA or PDOA, perfect synchronization is required. For the systems applying RSS, when time division multiplexing technique (TDM) is used to differentiate the light from different LEDs [6,7], synchronization is also

* Corresponding author at: Department of Electrical and Computer Engineering, National University of Singapore, 117576, Singapore.
E-mail address: a0105874@u.nus.edu (H. Zheng).

http://dx.doi.org/10.1016/j.optcom.2017.03.058
Received 20 December 2016; Received in revised form 23 March 2017; Accepted 25 March 2017

required among LEDs. As we know, in a commercial system, the synchronization is very difficult to realize, since the LED lamps are usually used only as transmitters, so they cannot receive synchronization signal. Thus, an asynchronous ranging technique is promising.

Although RSS is widely used in the indoor VLC-based positioning systems and the positioning accuracy of some reported indoor RSS-based visible light positioning systems can reach a few centimeters, however, most of them can only realize the 2-D localization [3,8,9]. In [6,10], positioning error of less than 3 cm has been reported in 3-D localization, however, besides the light sensor, an extra accelerometer or gyro-sensor is required for the system, which increases the positioning algorithm complexity. An asynchronous indoor positioning system (IPS) using VLC technology has been demonstrated in [9]. The Basic-framed slotted ALOHA (BFSA) protocol is used to solve the channel multiaccess problem. An accuracy of 5.9 cm can be achieved when locating the target receiver, with over 95% confidence. However, this work is only based on simulation in a typical line of sight (LOS) communication environment. In practical systems, a multi-path model is preferred since signals can be reflected by multiple surfaces. In our previous work [11], a positioning system is built and the experiment is carried out. The experiment results show that the average distance errors of x and y coordinates are 1.7 cm and 2.1 cm, respectively. However, this result is based on the experiment done in the central area of the test bed because on the margin area, the positioning error could become much worse. In this work, the experiment can be carried out on the whole test-bed. Not only 2-D but also 3-D positioning algorithms are developed and demonstrated. What is more, an error correcting algorithm (ECA) is also developed to improve the corner performance of the system. With the help of RSS measurements from the modulated LEDs, the asynchronous positioning with high accuracy is achieved in the experiments.

This paper is organized as follows. The system model and relevant notations are described in Section 2. Both the 2-D and 3-D positioning algorithms for indoor photodiode (PD)-based visible light positioning are proposed and the ECA is also introduced in Section 3. The experiment results are given in Section 4 and the conclusion is drawn in Section 5.

2. System configuration for indoor positioning

Fig. 1 describes the proposed the system configuration and Fig. 2 shows a picture of the test-bed environment we have built. Four LED lamps (LEDA, LEDB, LEDC, LEDD) are located on the ceiling. The receiver is a wide field of view (FOV) PD, which is OSD-15E manufactured by Centronic, as shown in Fig. 2. In order to distinguish the light signals from multiple LED lamps, different lamps are modulated by different center frequencies. Experiments are carried out at the space of 118.5 cm×100 cm×128.7 cm. When the receiver is placing in this space, signals from different LED lamps could be collected and then distinguished by applying Hamming filter to the received signals. RSS measurements can be translated into estimated distance between LED transmitters and the PD receiver and then trilateration algorithm is used to determine the position details of the receiver.

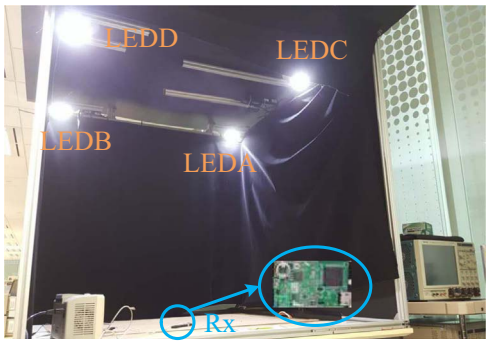

Fig. 2. Experiment set-up.

Four different carrier frequencies (12.5 kHz, 25 kHz, 50 kHz and 100 kHz) are assigned to four LED lamps, thus four hamming filters are required to separate signals from different lamps. Next are three steps to design the finite impulse response (FIR) filters.

1. According to the performance requirement, such as stopband attenuation and transitional bandwidth, the suitable windowing filter type and the filter order N are determined. Since the stopband attenuation as −53 dB and the transition bandwidth f_{Tr} as 5 kHz are chosen, Hamming filter can meet the design requirements and the designing of Hamming filter is simpler than other window filters, such as Hanning filter, Blackman–Harris filter and Cassell filter.
2. Generally, the impulse response for the FIR filter could be presented as: $h(n) = h_d(n)w(n)$ $(n = 0, 1, 2, \ldots, N-1)$. For Hamming filter, $N = 3.3f_s/f_{Tr}$, where f_s is the sample frequency. $w(n)$ is defined as: $w(n) = 0.54 - 0.46\cos(2n\pi)/(N-1)$. According to the expected fre-

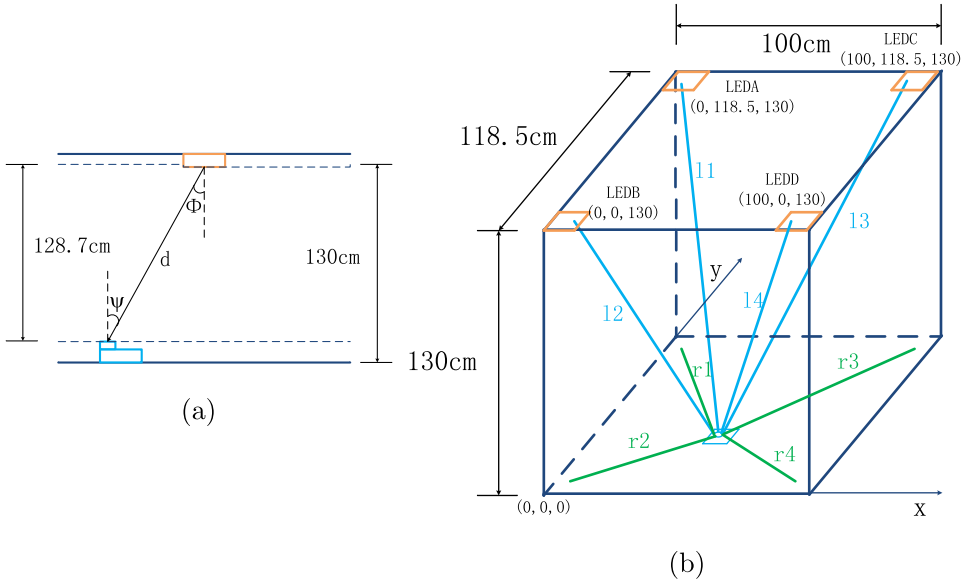

Fig. 1. (a) Side version of the system. (b) System structure diagram.

quency response $H_d(e^{j\omega})$, the impulse response $h_d(n)$ can be determined utilizing inverse Fourier transfer. In this way, the impulse response in our design is $h_d(n) = \frac{\sin((n-N)\times\omega_2) - \sin((n-N)\times\omega_1)}{(n-N)\pi}$, where ω_2 and ω_1 are the upper and lower cut-off angular frequency, respectively.

3. The signal after FIR filter can be presented as the convolution of the input signal and the impulse response: $y(n) = \sum_{k=0}^{N-1} h(k)x(n-k)$, where $y(n)$ is the signal after FIR filter while $x(n)$ is the signal before filtering.

LEDs can be generally modeled as Lambertian sources since the large beam divergence [12]. Denote P_t^i as the transmitted power difference between logical zeros and ones for the i-th transmission while P_r^i $(i = 1, 2, 3, 4)$ as the power difference at the receiver side. Without loss of generality, a simplified relationship between the transmitter and receiver power is [11,13]:

$$P_r^i = \frac{C}{d_i^2}\cos(\phi)\cos(\psi)P_t^i, \quad i = 1, 2, 3, 4, \tag{1}$$

where ψ is the angle of incidence, ϕ is the angle of irradiance, d_i is the distance between the i-th LED transmitter and PD receiver and C is a constant value, as Fig. 1(a) shows. Substituting the geometrical relationship $\cos(\phi) = \frac{h}{d}$ and $\cos(\psi) = \frac{h}{d}$ into Eq. (1), the following expression would be achieved:

$$P_r^i = \frac{Ch^2}{d_i^4}P_t^i. \tag{2}$$

Assuming that P_0^i is the reference received power just under the i-th lamp and the vertical distance between lamps and the receiver surface is h, the theoretical relationship between the normalized received power P_r^i/P_0^i and the distance d can be represented as:

$$P_r^i/P_0^i = \left(\frac{h}{d_i}\right)^4, \tag{3}$$

as depicted in Fig. 3 (a). Because the received power is fluctuated up and down slightly, P_0^i should be carefully selected with fine tuning for each lamp in order to match the modeling relationship. However, the theoretical power versus distance relationship could not match well with the experiment results, especially when the distance between the transmitter and receiver becomes larger, as Fig. 3(a) indicated.

In [14], the light intensity received by the PD is measured at various positions with the only variable is the different distances to the transmitter. With the help of the Matlab tool for nonlinear fitting named “nlintool” to fit the measured results by curves, [14] proposed the following mathematical model for the light power received by the light sensor:

$$P_r^i = \frac{C}{d_i^2}\cos(\phi)\cos(\psi)^n P_t^i, \quad i = 1, 2, 3, 4, \tag{4}$$

where n=1.4738, rather than n=1 in Eq. (1). This mathematical model also fits well with our experiment results, as shown in Fig. 3(b). This is because for the Centronic OSD-15E, the effective area is under the glass surface for a certain of depth. So part or all of the effective area will be in shadow of the opaque walls if the incidence angle of light is large enough, which will bring an additional drop of received light power. The theoretical relationship between the normalized received power and the ranges can be expressed as

$$P_r^i/P_0^i = \left(\frac{h}{d}\right)^{4.473}. \tag{5}$$

Thus, if the received power P_r^i from each LED is known at the receiver side, the distance between the lamp transmitter and the receiver can be calculated.

3. Indoor positioning algorithm

The target of the VLC positioning system is to estimate the location of the receiver. The Cartesian coordinate system is set up to determine the detail position of the receiver. As Fig. 1(b) shows the LEDA's coordinate is (0,118.5,130), the LEDB's coordinate is (0,0,130), the LEDC's coordinate is (100,118.5,130) and the LEDD's coordinate is (100,0,130). The length of the test-bed is 100 cm while the width is 118.5 cm.

3.1. Two-dimensional positioning

When moving the receiver on the receiver plane 1.3 cm above the test-bed because of the receiver's structure (Fig. 1(a)), the 2D positioning technique is applied. Because the height component is given in two-dimensional positioning, the receiver's position can be expressed as (x^e, y^e). According to the basic trilateration method, the positioning process can be carried out as follows:

- The receiver obtains signals from four LED lamps, and uses the received signal power to compute the distance between the transmitter and the receiver. Denote this distance from the LEDA, LEDB, LEDC, LEDD to the receiver projected on the receiver plane as r_i, $i = 1, 2, 3, 4$. The following distance equation can be established:

$$\begin{cases} \sqrt{(x^e)^2 + (width - y^e)^2} = r_1 \\ \sqrt{(x^e)^2 + (y^e)^2} = r_2 \\ \sqrt{(length - x^e)^2 + (width - y^e)^2} = r_3 \\ \sqrt{(length - x^e)^2 + (y^e)^2} = r_4 \end{cases} \tag{6}$$

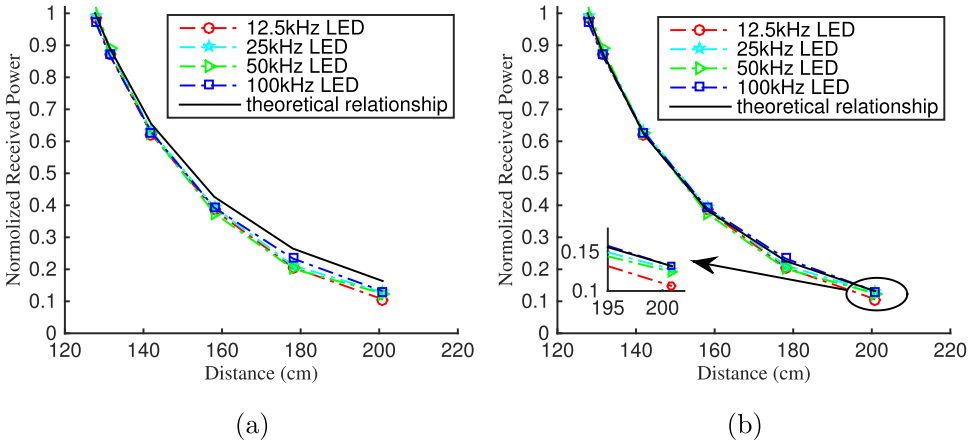

Fig. 3. The relationship between the normalized received power and distance: (a) n=1, (b) n=1.4738.

- Among the four signals, the three signals with higher normalized power are selected and used to calculate the projected ranges between the lamps and the receiver according to the relationship as described in Eq. (4), because as can be seen in Fig. 3(b), the larger distance will lead to larger misalignment between the modeling and realistic power–distance relationship. For example, when LEDA, LEDB, and LEDD are the three lights with relative stronger signal power when the receiver is at certain place. The equation system is as follows in this case:

$$\begin{cases} \sqrt{(x^e)^2 + (width - y^e)^2} = r_1 & \text{(a)} \\ \sqrt{(x^e)^2 + (y^e)^2} = r_2 & \text{(b)} \\ \sqrt{(length - x^e)^2 + (y^e)^2} = r_4 & \text{(c)} \end{cases} \tag{7}$$

From Eq. (7)(a) and (b), the y coordinate is determined as $\frac{r_2^2 - r_1^2 + width^2}{2 \times width}$ while from Eq. (7)(b) and (c), the x coordinate can be also expressed as $\frac{r_2^2 - r_4^2 + length^2}{2 \times length}$. Similar algorithm can be used to calculate the receiver's position on the whole receiver plane. The aforementioned process is also called linear least square estimation, which is widely used to provide the reliable localization service when there exist only small quantity of reference points [9,15,16].

3.2. Error correction algorithm in 2D positioning

Based on the above algorithm, the position detail of the receiver can be determined on the receiver plane with the knowledge of height component. However, because of the measurement error and fine tuning on P_0, sometimes, using the above-mentioned algorithm, the positioning error is not as small as expected, especially at the corners of the test-bed where relatively larger misalignment happens. In [17], a new algorithm is proposed, which could lessen the gap between the practical measurements and the actual values by varying the radius of the three circles. We use a similar algorithm, the so-called error correction algorithm (ECA), to improve the accuracy.

In theoretical model, a suggested assumption is made: there is no error when estimating the distance between the receiver and the transmitter. Thus, three circles used for trilateration are intersect at one point. This is not the case in the practical settings. In reality, the distance estimated is not accurate, leading to the case that three circles have intersected but it is not at one point. The projected distance estimated can be written in the following form:

$$r_i^e = r_i \pm \varepsilon \quad \text{or} \quad r_i = r_i^e \mp \varepsilon, \tag{8}$$

where r_i is the exact projected distance between the LEDs and PD, ε is the measurement dependent error. When ε is small, $r_i^e \approx r_i$, we will use original 2D positioning algorithm to get the solution of (x^e, y^e). However, when ε is too large to ignore, an ECA solution is drawing to compensate the measurement error. Take the case that signals from LEDA, LEDB and LEDD are three relative stronger signals as an example again. The largest measurement errors among different LEDs are the same in the example, the new system of equations are:

$$\begin{cases} \sqrt{(x^e)^2 + (width - y^e)^2} = r_1 \pm \varepsilon & \text{(a)} \\ \sqrt{(x^e)^2 + (y^e)^2} = r_2 \pm \varepsilon & \text{(b)} \\ \sqrt{(length - x^e)^2 + (y^e)^2} = r_4 \pm \varepsilon. & \text{(c)} \end{cases} \tag{9}$$

Because Eq. (9) cannot be solved directly, the Newton–Raphson (NR) method is utilized to do an approximation by considering ε as an error in the process of computing r_i^e. Eq. (9) can be expressed in an equivalent way as:

$$R_i \approx r_i \pm \varepsilon, \quad i = 1, 2, 4, \tag{10}$$

where

$$\begin{aligned} R_1 &= \sqrt{(x^e)^2 + (width - y^e)^2} \\ R_2 &= \sqrt{(x^e)^2 + (y^e)^2} \\ R_4 &= \sqrt{(length - x^e)^2 + (y^e)^2} \end{aligned} \tag{11}$$

Some notations need to be introduced first. At the k-th iteration, let $(x^{e[k+1]}, y^{e[k+1]}, \varepsilon^{[k+1]})$ be the value of (x^e, y^e, ε). Define the residual function $f_i(x^e, y^e, \varepsilon)$ as:

$$\begin{aligned} f_1 &= (x^e)^2 + (width - y^e)^2 - (r_1 \mp \varepsilon)^2 \\ f_2 &= (x^e)^2 + (y^e)^2 - (r_2 \mp \varepsilon)^2 \\ f_4 &= (length - x^e)^2 + (y^e)^2 - (r_4 \mp \varepsilon)^2 \end{aligned} \tag{12}$$

Then, the practical derivatives of f_i is defined as follows:

$$X'_i = \frac{\partial f_i}{x^e} \tag{13}$$

$$Y'_i = \frac{\partial f_i}{y^e} \tag{14}$$

$$E'_i = \frac{\partial f_i}{\varepsilon} \tag{15}$$

Because the NR method is an iterative algorithm, the residual function at the k-th iteration need to be defined:

$$f_i^{[k]} = R_i^{[k]} - r_i \mp \varepsilon. \tag{16}$$

To get a close enough solution to the true position, $f_i^{[k]}$ is expected to be close to zero. In the next step, according to Calculus techniques [18], the following expression is derived:

$$\begin{aligned} f_i^{[k+1]} - f_i^{[k]} \approx df_i = X'_i dx^e + Y'_i dy^e + E'_i d\varepsilon = X'_i(x^{e[k+1]} - x^{e[k]}) \\ + Y'_i(y^{e[k+1]} - y^{e[k]}) + E'_i(\varepsilon^{[k+1]} - \varepsilon^{[k]}) \end{aligned} \tag{17}$$

As the residual function value is expected to be zero in the next iteration, let $f_i^{[k+1]} = 0$. Thus, the above equation could be established as:

$$\begin{aligned} f_i^{[k]} + X'_i(x^{e[k]}, y^{e[k]}, \varepsilon^{[k]})(x^{e[k+1]} - x^{e[k]}) + Y'_i(x^{e[k]}, y^{e[k]}, \varepsilon^{[k]}) \\ (y^{e[k+1]} - y^{e[k]}) \quad + E'_i(x^{e[k]}, y^{e[k]}, \varepsilon^{[k]})(\varepsilon^{e[k+1]} - \varepsilon^{e[k]}) = 0. \end{aligned} \tag{18}$$

We can see that the value of $f_i^{[k]}$, X'_i, Y'_i and E'_i, $i = 1, 2, \ldots, m$, are determined at the end of the k-th iteration. According to the above analyst, the outlined algorithm of the NR method is presented:

1. Find the initial point for iteration, e.g.,
$$(x^{e[0]}, y^{e[0]}, z^{e[0]}, \varepsilon^{[0]}) = (0, 0, 0, 0). \tag{19}$$
2. Compute the residual function value of $f_i^{[k]}$ for $i = 1, 2, 3, 4$, as Eq. (12) shows.
3. Solve Eq. (17) for $(x^{e[k+1]}, y^{e[k+1]}, z^{e[k+1]}, \varepsilon^{[k+1]})$.
4. Continue until $f_i^{[k+1]}$ is small enough.
5. Let $k = k + 1$ and go to Step 2.

3.3. Three-dimensional positioning

When mobile phones are used for navigation in reality, the height of the receiver will vary because users can not only be adults with different heights, but also children, and even the disable and the aged sitting in the wheelchair. Thus, a 3-D localization algorithm is developed and discussed in 3-D space.

We choose the received power when the receiver is placed under the i-th LED lamp with the height h_0=91.2 cm as the reference received power P_{ref}^i. Because the radiation and incidence angles are kept at 0°, according to Eq. (4),

$$P_{ref}^{i} = \frac{C}{(h-h_0)^2}P_t^i. \tag{20}$$

In a similar way, when placing the receiver under the transmitters with h_{Rx} height, the received power P_0^{i*} can be derived as

$$P_0^{i*} = \frac{C}{(h-h_{Rx})^2}P_t^i. \tag{21}$$

Thus,

$$\frac{P_0^{i*}}{P_{ref}^{i}} = \left(\frac{h-h_0}{h-h_{Rx}}\right)^2. \tag{22}$$

As Fig. 4 shows, changing the vertical distance between the transmitter and the receiver by putting the receiver under each lamps with different heights, the relationship between the normalized received power and the vertical distance from the experiment results fit well with the theoretical one, which is indicated in Eq. (22).

When the receiver is placed with h_{Rx} height, by replacing $\cos(\phi)$ and $\cos(\psi)$ as $\frac{h-h_{Rx}}{d_i}$ in Eq. (4), the received power can be represented as

$$P_R^i = \frac{C\times(h-h_{Rx})^{n+1}}{d_i^{n+3}}P_t^i. \tag{23}$$

From Eqs. (20) and (23), the relationship between the normalized power and distance is as follows:

$$P_R^i = \frac{(h-h_0)^2(h-h_{Rx})^{n+1}}{d_i^{n+3}}P_{ref}^i. \tag{24}$$

The main steps of 3D positioning process is performed as follows:

- The receiver obtains signals from four LED lamps (LEDA, LEDB, LEDC and LEDD), and use the received signal power and h_{Rx} to express the ranges between the transmitter and the receiver as

$$d_i = \sqrt[n+3]{\frac{(h-h_0)^2(h-h_{Rx})^{n+1}P_{ref}}{P_R^i}} \tag{25}$$

according to Eq. (24). Let the estimated distance be d_i, four LEDs' coordinates be (x_i, y_i, z_i) as shown in Fig. 1(b), and the receiver's location (to be estimated) be (x^e, y^e, z^e). Then, the following distance equations can be written as:

$$\sqrt{(x_i-x^e)^2+(y_i-y^e)^2+(z_i-z^e)^2} = d_i. \tag{26}$$

- Among the four signals, the three signals with higher normalized power are selected and used to calculate d_i, according to the relationship as described in Eq. (25). For example, when LEDA, LEDC and LEDD are LED lights with relative stronger signal power when the receiver is at certain place. The equation system is as follows in this case:

$$\begin{cases} \sqrt{(x_1-x^e)^2+(y_1-y^e)^2+(z_1-z^e)^2} = d_1 \\ \sqrt{(x_3-x^e)^2+(y_3-y^e)^2+(z_3-z^e)^2} = d_3 \\ \sqrt{(x_4-x^e)^2+(y_4-y^e)^2+(z_4-z^e)^2} = d_4 \end{cases} \tag{27}$$

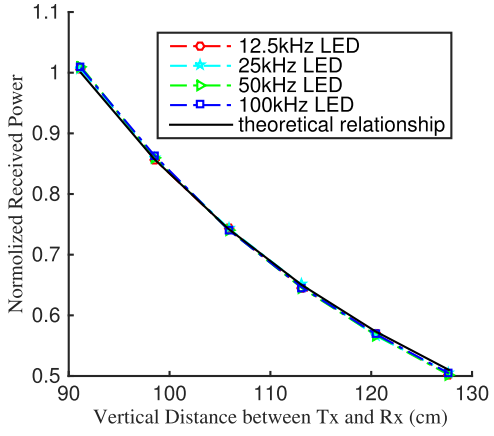

Fig. 4. Normalized received power versus vertical distance when placing the receiver under the transmitter.

The above equation system is derived from three spheres with the radius of the measured distance d_i and center of the reference points (x_i, y_i, z_i). Intersection between these three spheres is calculated as target position. The above equality holds if there is no error occurring when estimating the distance between the LED lamp and PD. However, this assumption may not work in practical settings. The above system of equations should change to the following optimization problem:

$$\begin{aligned} \text{minimize } f_1 &= (x_1-x^e)^2+(y_1-y^e)^2+(z_1-z^e)^2-d_1^2f_2 \\ &= (x_3-x^e)^2+(y_3-y^e)^2+(z_3-z^e)^2-d_3^2f_4 \\ &= (x_4-x^e)^2+(y_4-y^e)^2+(z_4-z^e)^2-d_4^2 \end{aligned} \tag{28}$$

In order to solve Eq. (28) using trust region method, the evaluation criterion σ is introduced:

$$\sigma = \underset{(x^e,y^e,z^e)}{\text{argmin}} f_1^2+f_2^2+f_4^2 \tag{29}$$

The detail process for the realization of trust region method is described as follows:

1. Assume h_{Rx}, $0 \le h_{Rx} \le h$ as the vertical height and substitute it into Eq. (25). Thus, $z^e = h - h_{Rx}$.
2. Estimate the coordinates (x^e, y^e, z^e) from solving Eq. (6).
3. Substitute the coordinates (x^e, y^e, z^e) into Eq. (29) to obtain the value of σ, and then update the trust region radius to minimize σ.
4. Iterate steps 1 to 2 in order to find the optimal estimated coordinates.
5. The value of h_{Rx} in step 1 is updated by the z^e optimized in step 3.

4. Experiment results and discussion

4.1. Two-dimensional positioning

As shown in Fig. 1, an experimental platform is built in order to evaluate the system performance. After applying 2-D positioning technique, the positioning error of x-axis and y-axis is indicated in Fig. 5(a) and (b), respectively. Comparing with the dotted lines, which are the accurate position values, the maximum x-axis and y-axis positioning errors are 6.17 cm and 2.50 cm, respectively. The average positioning errors of x-axis and y-axis are 1.18 cm and 1.25 cm, respectively. In Fig. 5(c), the disagreement between the estimated positioning points and real locations is demonstrated. The positioning error is quite small at most places of the receiver plane, which is acceptable. At four corners of the test-bed, relatively large disagreement happens. It is because when selecting the reference power, slight tuning is made in order to utmost match the experiment result to the theoretical model. However, this fine tuning leads to the misfit between the theoretical power versus distance relationship model and the real case for the points placed at the corner of the plane. Furthermore, the other LED lamps used to estimate the distance is a little far when the receiver is placed at the corner of the test-bed. As can be seen in Fig. 3(b), too far away distance between the transmitted and receiver is not a good news for the accurate positioning. What is more, the reflection of the wall is relatively larger at the corner of the test-bed, which will decrease the performance as well.

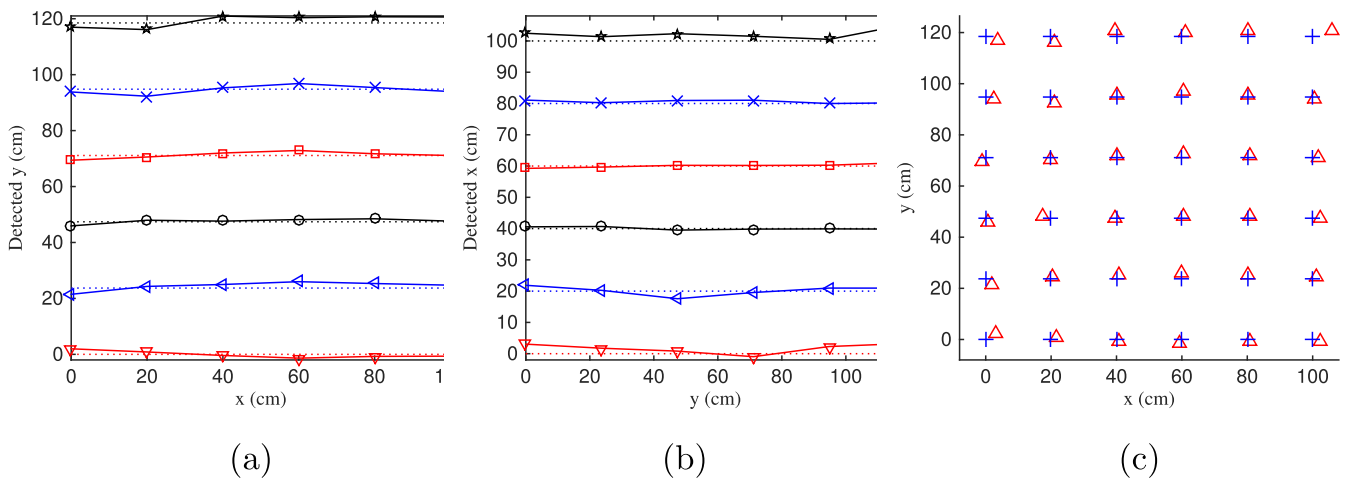

Fig. 5. Experiment results of 2-D positioning: (a) distance error at y-axis (dotted line is the accurate axis while full line is the estimated axis), (b) distance error at x-axis, (c) difference between the estimated position and real position (+ is the accurate position while △ is the estimated position).

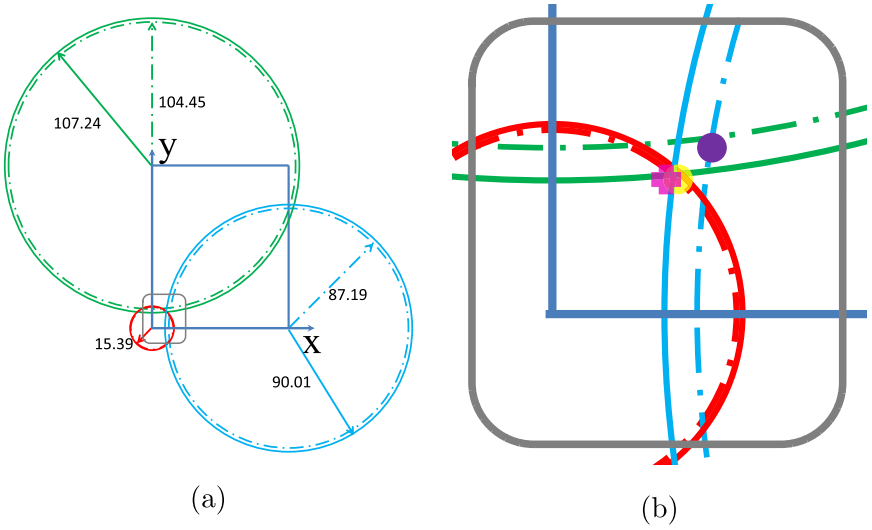

Fig. 6. The target position (10,11.85): (a) ECA estimation, (b) comparison between the estimated position with ECA and without ECA (fuchsia cross is the accurate position of the receiver, the yellow dot is the position estimated with ECA and the purple dot is the position estimated without ECA). (For interpretation of the references to color in this figure caption, the reader is referred to the web version of this paper.)

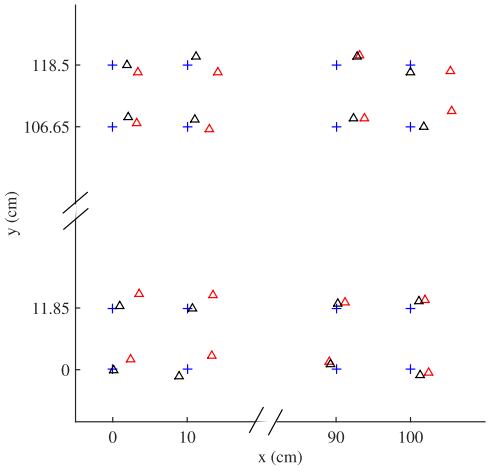

Fig. 7. Difference between the estimated position and real position (blue + is the accurate position, red △ is the estimated position without ECA and black △ is the estimated position with ECA). (For interpretation of the references to color in this figure caption, the reader is referred to the web version of this paper.)

4.2. Error correction algorithm in 2D positioning

In Fig. 5(c), it reveals that at most of the receiver plane, the positioning error is within 3 cm, where we assume small enough positioning error is achieved. However, at the corner of the receiver plane, the positioning error as large as 6.17 cm occurs, thus, the ECA is applied at these positions (corners of the receiver plane). An example is given in Fig. 6. When the receiver is placed at the point with coordinate (10, 11.85), the three LED lights used for localization is LEDA, LEDB and LEDD because they are nearer to the receiver and thus higher normalized power can be achieved. Then, the projected distance r_1, r_2 and r_4 are measured: r_1=104.45, r_2=15.39 and r_4=87.19. Based on this, using the original 2-D positioning algorithm, the estimated position coordinates are (13.55, 14.30) while after applying ECA to compensate the measurement error, the estimated position becomes (10.77, 11.80). Thus, the positioning error decreases from 4.31 cm to 0.77 cm. A more detail version is revealed in Fig. 6(b).

After ECA is applied, the positioning error at the corners becomes smaller observably. As shown in Fig. 7, the positioning performance is compared at four corners. With the help of ECA, the estimated position becomes closer to the real position compared with the estimated results without ECA. At the lower left corner, the average positioning error is

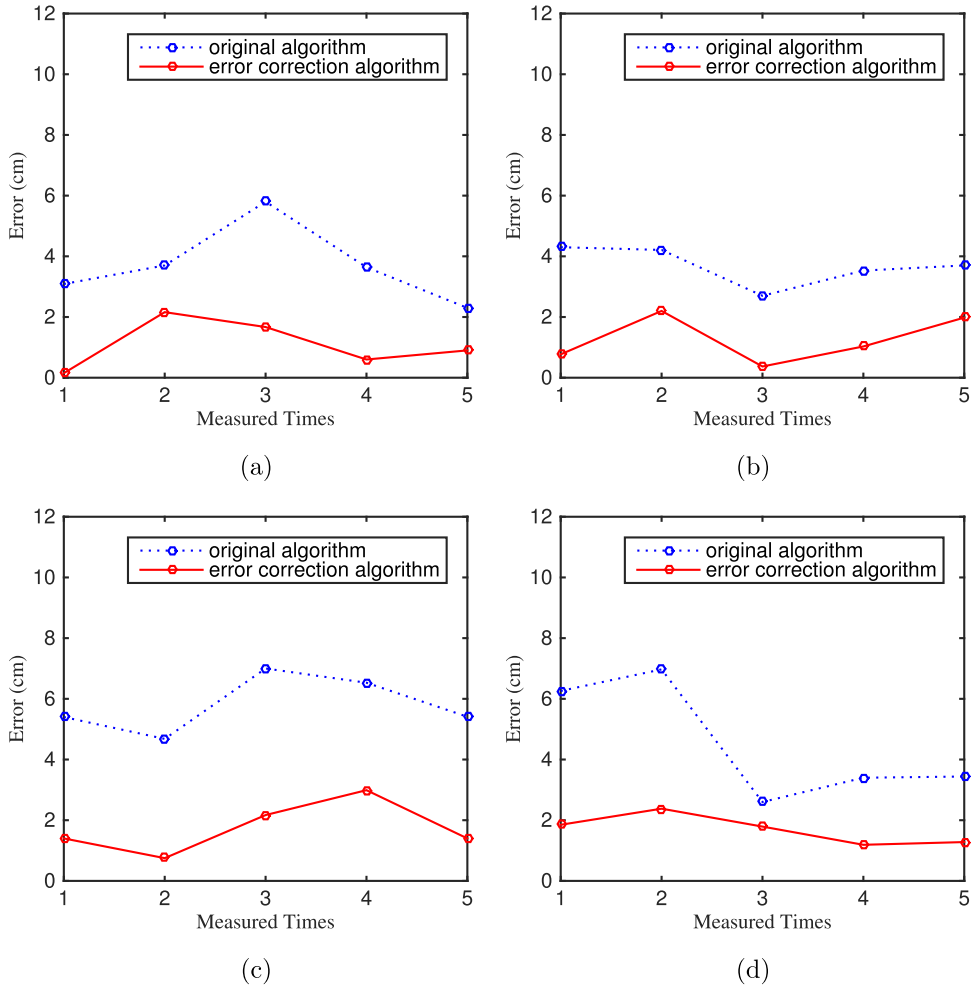

Fig. 8. Comparison between experiment results with ECA and without ECA: (a) target (0, 0), (b) target (10, 11.85), (c) target (100, 118.5), (d) target (100, 106.65).

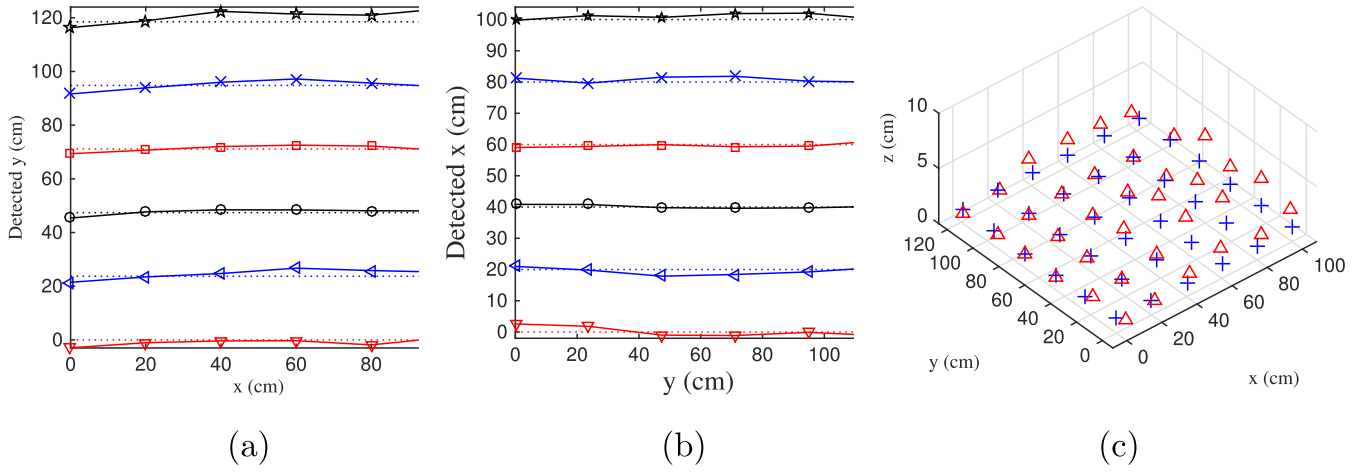

Fig. 9. Experiment results of 3-D positioning: (a) distance error at *y*-axis (dotted line is the accurate axis while full line is the estimated axis), (b) distance error at *x*-axis, (c) difference between the estimated position and real position (+ is the accurate position while △ is the estimated position).

as large as 4.06 cm without ECA while it decreases to 0.90 cm with ECA. At the upper left corner, after applying ECA, the average positioning error decreases from 3.64 cm to 2.03 cm. For the upper right corner, the original algorithm leads to 4.87 cm average positioning error while the ECA algorithm leads to only 1.87 cm. For the lower right corner, the positioning accuracy is also improved. The estimated positioning error is 2.09 cm without ECA while 1.40 cm with ECA.

In Fig. 8, the performance details at four example positions for the cases with and without ECA are shown. At the position with coordinates (0, 0), the mean positioning error of five times is 3.71 cm using the original 2-D positioning algorithm while it decreases to 1.10 cm after applying ECA. Around the position (0, 0), such as the point at (10, 11.85), the mean positioning error is decreased from 3.69 cm to 1.27 cm with the help of ECA. The other two examples we have shown

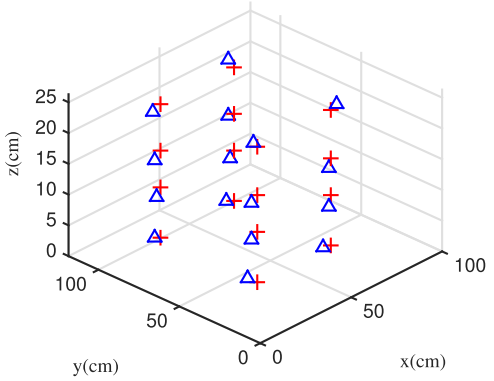

Fig. 10. Experiment results of difference between the estimated position and real position (+ is the accurate position while △ is the estimated position).

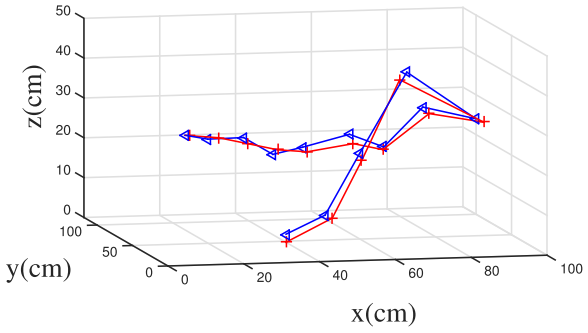

Fig. 11. Experiment results of random tracking points in 3D space (+ is the accurate position while △ is the estimated position). (For interpretation of the references to color in this figure caption, the reader is referred to the web version of this paper.)

are at (100, 118.5) and (100, 106.65). For the test point with coordinate (100, 118.5), the average position error is reduced from 5.80 cm to 1.74 cm while at (100, 106.65) the positioning error is decreased from 4.53 cm to 1.70 cm.

4.3. Three-dimensional positioning

After applying 3-D positioning technique, the positioning error on the receiver plane with 1.3 cm height is demonstrated in Fig. 9. Comparing with the accurate position values, which is indicated using the dotted lines, the maximum positioning errors of x-axis and y-axis are 2.58 cm and 5.00 cm, respectively, as shown in Fig. 9(a) and (b). The mean positioning errors of x-axis and y-axis are 0.90 cm and 1.54 cm, respectively. In Fig. 9(c), the disagreement between the estimated positions and the real locations is shown in 3-D space. The maximum vertical positioning error is 2.20 cm while the mean vertical error is 0.66 cm.

After picking up several points with different vertical distances, Fig. 10 is drawn. The accurate x and y coordinates of the four points selected are (30, 94.8), (30, 35.55), (70, 94.8), and (70, 35.55). The four altitude levels chosen are 1.3 cm, 9.4 cm, 15.4 cm and 23.1 cm. On the 1.3 cm height receiver plane, the mean error of x-axis of these four points is 2.44 cm while the mean error of y-axis is 2.00 cm. The average distance error is 2.97 cm in 3-D space. For the case when the altitude level is 9.4 cm, the mean error of x-axis is 1.58 cm while the mean error of y-axis is 0.87 cm. The average positioning error in 3-D is 2.90 cm on the 9.4 cm height plane. On the receiver plane with 15.4 cm height, the average error of x-coordinate is 1.49 cm while for y-coordinate is 1.46 cm. The 3-D distance error in space is 3.00 cm. When the altitude height increases to 23.1 cm, the mean error of x-axis is 1.52 cm while the y-axis mean error is 0.15 cm. The average distance error is 2.68 cm in 3-D, which is still within 3 cm.

A random moving path is generated in the test-bed with 13 points. The experiment results reflecting the difference between the real reference points and the estimated points are shown in Fig. 11.

The actual path is indicated using the red line while the estimated one is indicated by the blue line. The maximum positioning error is 2.98 cm and the average difference between the calibration points and estimated ones is 2.09 cm.

In order to show the results clearer, Fig. 11 is separated into the horizontal and vertical views. As can be seen in Fig. 12(a), the estimated points are slightly deviated from the true tracking path from the view of horizontal. The maximum deviation is 2.25 cm while the mean difference is 1.23 cm. As reflected in Fig. 12(b), the estimated points are close to the calibration points from the vertical view. The maximum deviation of the vertical side is 2.97 cm and the mean deviation is only 1.48 cm. These results match well with the conclusion that the average distance error is within 3 cm in 3-D space.

5. Conclusion

We demonstrated an indoor positioning system making use of light emitting diode lamps. In order to distinguish lights from different light sources, FIR filters are used at receiver side. A pre-determined normalized received power–distance relationship is wielded to calculate the distance based on the received power. A 2-D positioning algorithm was applied to determine the receiver's coordinates. In the experimental space of 100 cm×118.5 cm×128.7 cm, the mean distance errors of x-axis and y-axis are 1.18 cm and 1.25 cm, respectively. The error correcting algorithm was used to decrease the positioning errors at the corners of the receiver plane, where relatively large positioning errors happen. The average positioning error at the four corners decreases from 3.67 cm to 1.55 cm after applying ECA. A 3-D positioning algorithm was also developed and demonstrated. The mean positioning error of x-axis, y-axis and vertical are 0.90 cm, 1.54 cm and 0.66 cm on the plane with 1.3 cm height, respectively. The experiment results of error distribution on four altitude levels were presented and the average distance errors on each test plane are all within 3 cm. The performance of four altitude levels is similar. What is more, a random

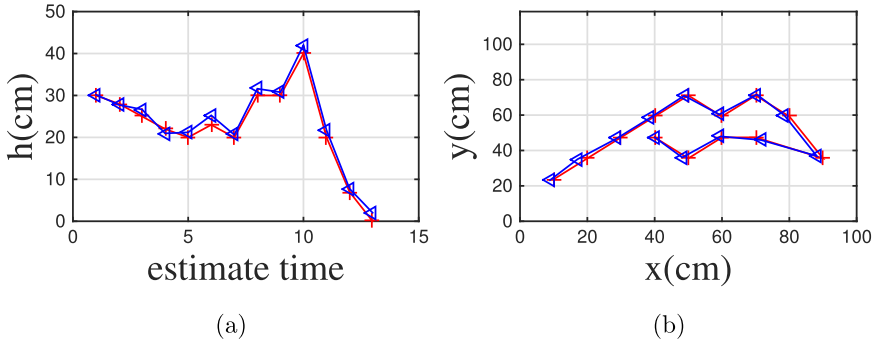

Fig. 12. Vertical and horizontal experiment results in 3D space: (a) vertical result, (b) horizontal result.

track is also plotted to reflect the positioning deviation and the results show that the positioning errors of all experiment points are within 3 cm. The proposed localization scheme could be a promising candidate in the future indoor localization systems, especially in LED lighting environments.

Acknowledgment

The authors would like to thank the supports of A*STAR SERC Project 1420200044 and HKPU Grant 1-ZE5K.

References

[1] D. Dardari, P. Closas, P.M. Djurić, Indoor tracking: theory, methods, and technologies, IEEE Trans. Veh. Technol. 64 (4) (2015) 1263–1278. http://dx.doi.org/10.1109/TVT.2015.2403868.
[2] M. Yasir, S.-W. Ho, B.N. Vellambi, Indoor position tracking using multiple optical receivers, J. Lightwave Technol. 34 (4) (2016) 1166–1176. http://dx.doi.org/10.1109/JLT.2015.2507182.
[3] H.-S. Kim, D.-R. Kim, S.-H. Yang, Y.-H. Son, S.-K. Han, An indoor visible light communication positioning system using a rf carrier allocation technique, J. Lightwave Technol. 31 (1) (2013) 134–144. http://dx.doi.org/10.1109/JLT.2012.2225826.
[4] S.-Y. Jung, S. Hann, C.-S. Park, Tdoa-based optical wireless indoor localization using led ceiling lamps, IEEE Trans. Consum. Electron. 57 (4) (2011) 1592–1597. http://dx.doi.org/10.1109/TCE.2011.6131130.
[5] K. Panta, J. Armstrong, Indoor localisation using white leds, Electron. Lett. 48 (4) (2012) 228–230. http://dx.doi.org/10.1049/el.2011.3759.
[6] M. Yasir, S.-W. Ho, B.N. Vellambi, Indoor positioning system using visible light and accelerometer, J. Lightwave Technol. 32 (19) (2014) 3306–3316. http://dx.doi.org/10.1109/JLT.2014.2344772.
[7] Z. Zhou, M. Kavehrad, P. Deng, Indoor positioning algorithm using light-emitting diode visible light communications, Opt. Eng. 51 (8) (2012). http://dx.doi.org/10.1117/1.OE.51.8.085009 085009-1.
[8] W. Zhang, M. Kavehrad, A 2-d indoor localization system based on visible light led, in: 2012 IEEE Photonics Society Summer Topical Meeting Series, 2012. http://dx.doi.org/10.1109/PHOSST.2012.6280711.
[9] W. Zhang, M.S. Chowdhury, M. Kavehrad, Asynchronous indoor positioning system based on visible light communications, Opt. Eng. 53 (4) (2014) 045105. http://dx.doi.org/10.1117/1.OE.53.4.045105.
[10] S.-H. Yang, H.-S. Kim, Y.-H. Son, S.-K. Han, Three-dimensional visible light indoor localization using aoa and rss with multiple optical receivers, J. Lightwave Technol. 32 (14) (2014) 2480–2485. http://dx.doi.org/10.1109/JLT.2014.2327623.
[11] H. Zheng, Z. Xu, C. Yu, M. Gurusamy, Indoor three-dimensional positioning based on visible light communication using hamming filter, in: Signal Processing in Photonic Communications, Optical Society of America, Vancouver Canada, 2016, p. SpM4E-3. http://dx.doi.org/10.1364/SPPCOM.2016.SpM4E.3.
[12] F.R. Gfeller, U. Bapst, Wireless in-house data communication via diffuse infrared radiation, Proc. IEEE 67 (11) (1979) 1474–1486. http://dx.doi.org/10.1109/PROC.1979.11508.
[13] M. Yasir, S.-W. Ho, B.N. Vellambi, Indoor localization using visible light and accelerometer, in: 2013 IEEE Global Communications Conference (GLOBECOM), IEEE, Hilton Atlanta Atlanta, GA, USA, 2013, pp. 3341–3346. http://dx.doi.org/10.1109/GLOCOM.2013.6831588.
[14] S.-W. Ho, J. Duan, C.S. Chen, Location-based information transmission systems using visible light communications, Trans. Emerging Tel. Tech. 28 (1) (2017) e2922. http://dx.doi.org/10.1002/ett.2922.
[15] W. Gu, M. Aminikashani, P. Deng, M. Kavehrad, Impact of multipath reflections on the performance of indoor visible light positioning systems, J. Lightwave Technol. 34 (10) (2016) 2578–2587. http://dx.doi.org/10.1109/JLT.2016.2541659.
[16] A. Noroozi, M.A. Sebt, Weighted least squares target location estimation in multi-transmitter multi-receiver passive radar using bistatic range measurements, IET Radar Sonar Navig. 10 (6) (2016) 1088–1097. http://dx.doi.org/10.1049/iet-rsn.2015.0446.
[17] M.M. Zaniani, A.M. Shahar, I.A. Azid, Trilateration target estimation improvement using new error correction algorithm, in: 2010 18th Iranian Conference on Electrical Engineering, 2010. http://dx.doi.org/10.1109/IRANIANCEE.2010.5507021.
[18] G.B. Thomas, R.L. Finney, Calculus and Analytic Geometry, Addison Wesley Publishing Company, 1984.